AraOptical Testbed: Design, Field Trials, and Channel Analysis of Long-range FSOC System with COTS Transceivers

Xun Li, Ataberk Atalar, Md Nadim, Sarath Babu, Ozan Berk Boyraz, Christian Joseph Margison, Mustafa Mert Bayer, Arsalan Ahmad, Daji Qiao, Hongwei Zhang, and Ozdal Boyraz, *Senior Member, Optica*

***Abstract*—This paper presents *AraOptical*, a 10.15 km rural free-space optical communication (FSOC) testbed designed using commercial off-the-shelf (COTS) 10G SFP+ transceivers and integrated into the ARA wireless living lab. The system features a multi-level autonomous alignment algorithm and real-time link monitoring, enabling stable high-throughput communication in dynamically varying atmospheric conditions. A continuous 2-hour UDP-based bit rate test was conducted, and environmental data were logged to investigate turbulence-induced impairments. A two-stage polynomial regression approach was developed to estimate the refractive index structure parameter (C_n^2) from weather station data and predict link throughput by combining one-minute block-averaged received power with the Rytov variance predicted from the measured meteorological data. The proposed model achieved $R^2 = 89.92\%$ for turbulence estimation and $R^2 = 62.22\%$ for throughput prediction. Our results demonstrate the feasibility of using in-situ environmental sensing and data-driven models to characterize and predict FSOC performance under real-world conditions.**

***Index Terms*—Free space optical communication, auto-alignment, algorithm, COTS SFP+ transceiver, turbulence modeling, bit rate prediction**

I. Introduction

FREE-SPACE optical communication (FSOC) has emerged as a critical enabler for next-generation high-speed communication systems. While traditional fiber-optic networks have long been served as the backbone of broadband infrastructure, their reach is constrained by the physical limitations of fiber deployment [1], [2], [3] and high capital expenditures relative to potential revenue, especially in rural regions. FSOC offers a compelling alternative by transmitting optical signals directly through the atmosphere without the need for a physical medium, thus enabling flexible and cost-effective deployment in urban, rural, aerial, and satellite networks [4]. Beyond serving as a wireless extension to fiber backbones, FSOC is increasingly viewed as a strategic solution to meet the stringent requirements of future communication systems [5].

In particular, the ever-increasing demand for ultra-high bandwidth and ultra-low latency communication systems, especially with the rise of data-intensive 5G/6G applications, is pushing the limits of radio frequency (RF) systems, which are inherently bandwidth-constrained and spectrum-regulated [1], [6]. FSOC addresses the fundamental limitations of current wireless technologies to fulfill this strategic role. Specifically, FSOC provides several key advantages: license-free spectrum, high data rates, low power consumption, immunity to electromagnetic interference, and strong security characteristics [7]. Moreover, FSOC can be seamlessly integrated with existing optical fiber infrastructures, acting as a wireless extension to fiber-optic backbones and bridging the last/middle-mile gap [8], [9].

Despite its promising advantages, long-range FSOC links face major performance barriers due to environmental and mechanical instabilities. Atmospheric turbulence introduces intensity scintillation, beam wandering, and wavefront distortion, leading to random fluctuations in received power and potential link outages [10]. On the other hand, temporal variations in temperature, pressure, and humidity induce fluctuations in the refractive index of air, causing coherence time to vary from seconds to minutes [11]. These effects significantly degrade the coupling efficiency into the optical fiber at the receiver, especially under tight alignment constraints.

To date, fiber optical communication has been well established over the past four decades, encompassing many active and passive technologies. For instance, transceivers are developed to enable data transmission rates of up to 800 Gbps over distances of 1000 km [12]. However, their suitability for FSOC is questionable. In this paper, we investigate an FSOC system that employs COTS transceivers originally developed for fiber-optic networking within a mature and well-supported industrial ecosystem. However, these transceivers are not inherently designed to withstand the turbulent conditions of free-space channels, where comparable industrial support for FSOC-specific transceivers remains limited [13]. As a result, the use of these transceivers in FSOC is constrained by several technical limitations, including fixed receiver sensitivity, poor adaptability to spatial intensity fluctuations, vulnerability to pointing errors, and the lack of weather-resilient adaptive control mechanisms [14]. Consequently, significant performance degradation may occur when COTS SFP+s are directly employed in FSOC systems without additional system-level enhancements.

To address these challenges, researchers have proposed a range of adaptive techniques, including automated beam align-

Xun Li, Ataberk Atalar, Ozan Berk Boyraz, Christian Joseph Margison, Mustafa Mert Bayer, and Ozdal Boyraz are with the Department of Electrical Engineering and Computer Science, University of California, Irvine, CA, 92697 USA e-mail: (xunl12@uci.edu, aatalar@uci.edu, ozan.berk@uci.edu, margisoc@uci.edu, bayerm@uci.edu, oboyraz@uci.edu).

Md Nadim, Sarath Babu, Arsalan Ahmed, Daji Qiao, and Hongwei Zhang are with the Department of Electrical and Computer Engineering, Iowa State University, Ames, IA 50011 e-mail:(nadim@iastate.edu, sarath4@iastate.edu, aahmad@iastate.edu, daji@iastate.edu, hongwei@iastate.edu)

ment, neural network-based turbulence compensation, and real-time control of Erbium-Doped Fiber Amplifier (EDFA) and Adaptive Optics (AO) modules [15], [16], [17]. However, the practical implementation of these solutions often remains complex, costly, or constrained by computational and latency constraints. Meanwhile, coherent optics, which have proven highly effective in long-haul fiber systems, are gaining increasing attention for FSOC applications due to their superior receiver sensitivity and advanced digital signal processing capabilities that enhance tolerance to turbulence-induced distortions [17]. Nevertheless, achieving robust, low-latency, and high-throughput FSOC communication over extended distances still demands careful system-level co-design that integrates optics, control, and network-layer intelligence.

In this work, we present *AraOptical*, a publicly available FSOC system deployed in the rural agricultural region of Ames, Iowa, spanning a distance of 10.15 km. The *AraOptical* link operates at 194 THz in the C-band and is equipped with commercially available switches and Small Form-Factor Pluggable Plus (SFP+) transceivers. The *AraOptical* telescope is integrated with a beacon alignment system that employs a self-alignment algorithm to ensure precise link alignment. Furthermore, we integrate *AraOptical* as a key component of the ARA wireless living lab [18], an at-scale wireless testbed in Central Iowa for advanced wireless research, thereby establishing a pioneering heterogeneous wireless x-haul platform that facilitates experimentation with long-range FSOC systems in real-world rural environments. Using the *AraOptical* platform, we collect extensive firsthand data, allowing a detailed analysis of scintillation effects and misalignment on the effective bit rate. The *AraOptical* platform is publicly available for experimental demonstrations of novel algorithms and transceiver architectures designed to enhance the robustness of FSOC systems, as well as for custom heterogeneous integration experiments.

The key contributions of this work include: (1) development and validation of a self-alignment algorithm, (2) deployment and characterization of a 10.15 km FSOC link with commercially available SFP+ transceivers in real atmospheric conditions, and (3) comprehensive analysis of atmospheric effects on link performance using extensive field measurements.

II. Experimental Setup

Fig. 1 shows an overview of the 10.15 km bidirectional FSOC link, deployed using *AraOptical* telescope terminals. The two optical nodes are installed in Ames, Iowa: one on the roof of Residence Hall, a student residence building, and the other on a pole at Agronomy Farm. Each terminal features a custom optomechanical housing that encloses the optical components and supports dual-axis motorized steering for beam alignment. A wavelength-division multiplexer (WDM) is used to combine the signal and beacon lasers into a shared optical path, which is then launched through a collimator to ensure spatial co-propagation and minimize the boresight error between the beacon and signal beams. Key components, including avalanche photodiodes (APDs), CMOS cameras, and dual-axis motorized steering units, are integrated to enable autonomous beam alignment and robust long-distance connectivity.

Meanwhile, the FSOC link is subject to atmospheric turbulence, which induces beam wander, scintillation, and wavefront distortion, potentially degrading the received signal power and coupling efficiency. These effects are particularly pronounced over long horizontal terrestrial paths, where temperature gradients and wind variations are significant. To monitor the local environmental conditions in real time, weather stations and disdrometers are installed at both Wilson Hall and Agronomy Farm sites. The stations continuously record parameters such as wind speed, temperature, humidity, and barometric pressure, which are later correlated with optical link performance metrics.

A. Hardware Design

The overall architecture of the *AraOptical* system is illustrated in Fig. 1. Each terminal is equipped with 16×10G-Base-ZR dense wavelength-division multiplexing (DWDM) SFP+ transceivers (ProLabs), operating at distinct ITU C-band wavelengths over single-mode fiber (SMF) and interfaced through a Juniper ACX710 metro router. The transceivers are directly connected to a DWDM module, which performs wavelength multiplexing and demultiplexing for both transmission and reception.

A fiber optical circulator is then employed to enable bidirectional signal routing through a shared telescope aperture while maintaining separate internal transmit and receive paths. To provide sufficient optical launch power for long-range terrestrial free-space links, an erbium-doped fiber amplifier (EDFA) with a saturated output power of 33 dBm is placed before free-space transmission. On the receiver side, a 98/2 optical splitter taps 2% of the received signal to an optical power meter for real-time monitoring and feedback control. The remaining 98% of the signal is amplified by a low-noise pre-amplifier (LNA, LiComm SFP+-EDFA), which boosts the optical power to 0 dBm via an automatic power control (APC) mechanism prior to wavelength demultiplexing and detection by the SFP+ receivers. Given the LNA minimum input threshold of -25 dBm, the optical backbone is configured to intentionally route residual transmitter-to-receiver crosstalk from the circulator into the LNA, ensuring continuous amplifier operation. This design mitigates signal degradation and compensates for power fluctuations caused by atmospheric turbulence and pointing misalignment. Free-space transmission is realized using a collimator with a divergence angle of 35 µrad to minimize geometric propagation losses.

The self-alignment beacon system, on the other hand, has been developed to mitigate the reductions in fiber coupling efficiency caused by incidence angle mismatches, beam walk-off, and weather-induced turbulence. As shown in Fig. 1, a 980 nm beacon laser is multiplexed with the signal beam using a WDM, ensuring that both beams remain aligned. Since the collimator is optimized for signal transmission in the C-band, the beacon beam experiences higher divergence, which relaxes the angular precision required during initial alignment and facilitates easier acquisition. Fig. 2 provides a visualization

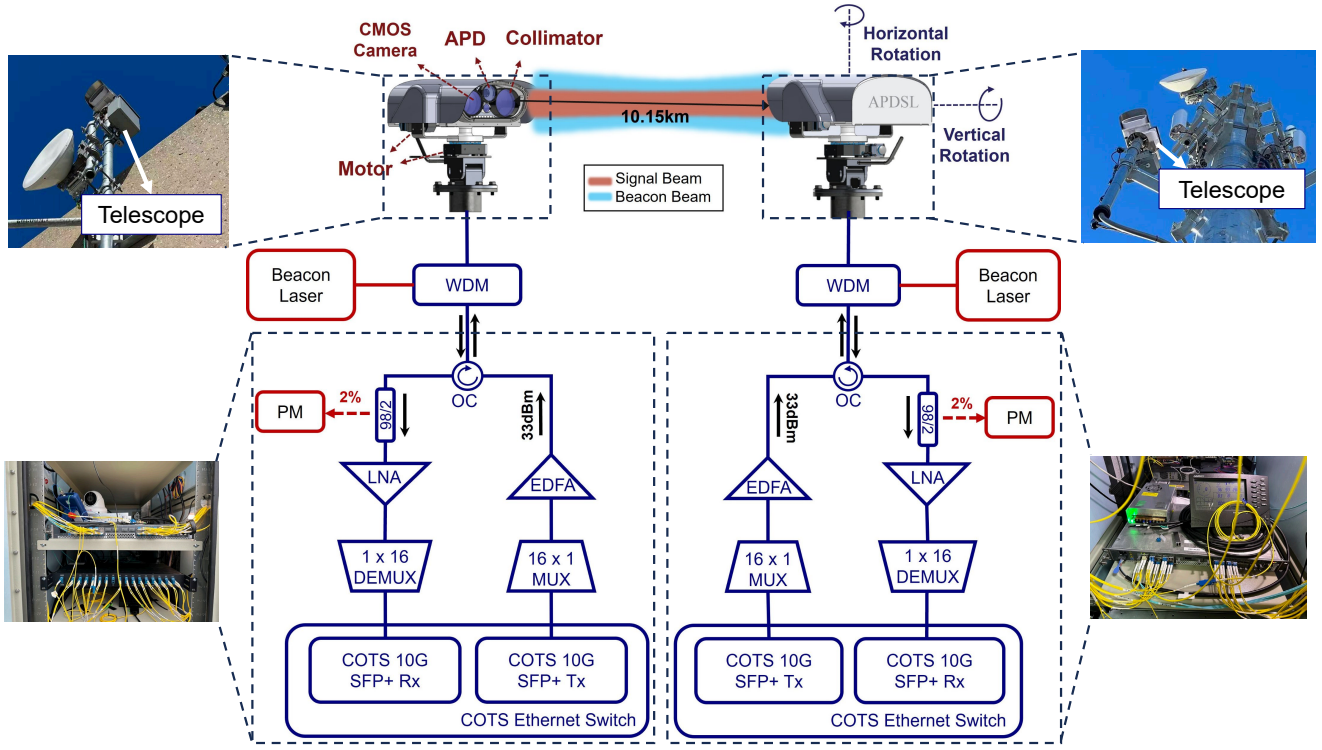

Fig. 1. Architecture of the *AraOptical* system, illustrating a multiplexed FSOC channel equipped with an automated multi-layer alignment feedback loop based on CMOS imaging, APD detection, and signal-power-based ultra optimization; SFP+, small form-factor pluggable plus transceiver; MUX/DEMUX, multiplexer/demultiplexer; EDFA, Erbium-doped fiber amplifier; LNA, low-noise optical amplifier; OC, optical circulator; PM, power meter; WDM, wavelength division multiplexer; APD, avalanche photodiode; CMOS Camera, complementary metal-oxide-semiconductor camera.

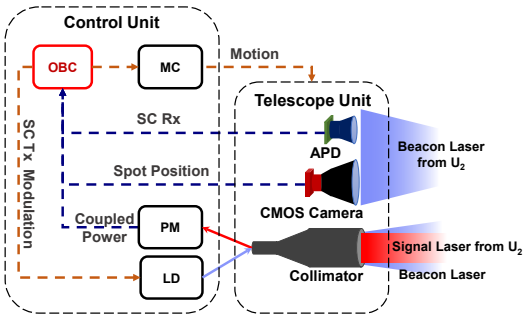

Fig. 2. Architecture of the AraOptical multi-stage alignment system with a closed-loop feedback structure; OBC, on-board computer; MC, motor controller; SC: supervisory channel; PM, power meter; LD, beacon laser diode; APD, avalanche photodiode; CMOS Camera, complementary metal–oxide–semiconductor camera.

of the self-alignment system, which is supported by a custom-designed mechanical housing and employs two high-resolution motorized rotational stages, each capable of 0.23 µrad per micro-step, enabling precise horizontal and vertical adjustments of the telescope. In the beacon receiver system, the APD has a large detection area of 100 mm^2 and is placed behind a 50 mm double-convex lens, which provides the most *coarse* alignment with the largest angle of view up to $\pm 6.5°$. The *fine* alignment is then accomplished using a 24 mm^2 CMOS camera with a pixel size of 3.45 µm $\times$ 3.45 µm and a 75 mm aspheric lens, which detects the pixel-to-pixel movement of the focused beacon beam when the incidence angle deviates, yielding an angular resolution of 30 µrad [19]. Before conducting field tests, two nodes have been aligned perfectly on the hallway (nearly 45 m), the CMOS camera pixel coordinates for perfect alignment are recorded. This recording is used as a reference point to minimize the searching process. After the power meter detects a threshold power, the algorithm performs an ultrafine scanning to optimize the fiber coupling efficiency. In short, the self-alignment algorithm processes data from the APD (coarse alignment), CMOS camera (fine alignment), and power meters (ultra-fine alignment) in the signal branch to dynamically control the motorized stages, forming a closed-loop feedback system that continuously ensures stable and robust connectivity.

B. Control Algorithms

AraOptical is equipped with a multi-level auto-alignment system designed to restore and maintain the optimal alignment of the FSOC link under varying atmospheric and mechanical disturbances, including the effects of vibration, scintillation, and beam wandering. To facilitate initial handshaking and alignment coordination between the two terminals, the beacon system incorporates a low-rate sub-communication channel. The beacon laser, modulated using an on-off keying (OOK) scheme at 1 Mbps, serves as a management channel for transmitting alignment commands from the control computer. At the receiver end, the beacon signal is detected by an avalanche photodiode (APD) and digitized via an analog-to-digital converter (ADC) connected to the control computer.

Clock and data recovery are then performed digitally, allowing the control computer to extract alignment information and initiate appropriate alignment responses.

The auto-alignment process operates across three stages: *coarse*, *fine*, and *ultra-fine*, each controlling two orthogonal axes of the motorized steering system. As illustrated in Fig. 3, the process begins with coarse alignment, which performs a wide-range raster scan to bring the received beam within the field-of-view of the receiver. During this stage, the system monitors for successful recovery of the beacon handshake signal. Once communication is established, a second coarse raster scan is executed to maximize the APD signal, indicating spatial overlap and temporal synchronization. Following successful coarse alignment, the algorithm enters the fine alignment phase. Here, a linear scan is used to center the beacon spot on the CMOS camera image plane, providing precise angular correction of the beam's incident direction. Once the beam is centered, the system proceeds to the ultra-fine alignment stage. In the ultra-fine phase, the system uses feedback from the received signal power—monitored via the 2% tap of an optical splitter in the receiver branch—to optimize fiber coupling. The built-in power meter of the transceiver typically offers a minimum detectable power of only 0.1 µW with a refresh interval of approximately 2 s. To address this limitation, the *AraOptical* system incorporates an external high-sensitivity power meter, capable of detecting power levels down to the picowatt range with real-time response. A localized raster scan is initiated when the received power exceeds a predefined threshold (e.g., 1 nW), followed by a linear scan to fine-tune the alignment. Due to the mechanical backlash in the stepper-motor-driven actuators, scan patterns involving frequent direction reversals may introduce positioning errors during ultra-fine alignment. To mitigate this effect, linear scans along fixed directions are employed to reduce backlash-induced uncertainty and to more reliably identify the global maximum of the coupling efficiency within a confined search region, even in the presence of power fluctuations. Once the peak coupling is achieved, the system transitions into a steady-state tracking and maintenance mode, in which received power is continuously monitored to maintain stable FSOC operation. The implementation of these alignment algorithms is supported by an integrated software framework that coordinates sensing, actuation, and network-level control between the two terminals. After alignment is established, the motor home position and the corresponding CMOS pixel coordinates are stored as a calibrated reference, enabling automatic re-alignment in the event of vibration-induced disturbances or long-term motor drift. This calibration is also essential for compensating residual boresight offsets between the tracking CMOS camera and the communication optical path.

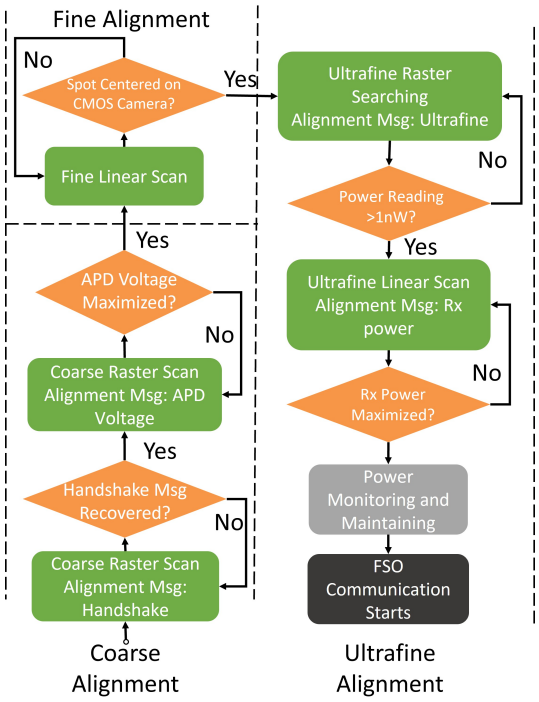

Fig. 3. Multi-stage alignment process of the *AraOptical* FSOC system showing coarse, fine, and ultrafine alignment loops that progressively maximize APD voltage, center the beam spot, and optimize received power before initiating communication.

C. Software and System Integration

In addition to the hardware and control algrorithm design, the *AraOptical* platform incorporates an integrated software framework that coordinates real-time monitoring, control, and data acquisition across both terminals. The framework was developed to ensure autonomous operation, rapid recovery, and reproducible long-term field measurements. It coordinates different subsystems such as the motorized alignment stages, power meters, environmental sensors, and optical amplifiers through a unified network-based control [20].

The software architecture follows a modular client–server design. Each terminal hosts a local control computer running a Python-based backend built on the *Flask* framework. The backend exposes RESTful interfaces accessible through HTTP requests, allowing operators or higher-level scripts to execute commands and query system status remotely. These interfaces abstract the low-level serial and GPIO communications required to control actuators and sensors, enabling distributed automation and safe parallel operation of multiple components within the system.

A dedicated process continuously collects telemetry from the photodiode power meters, CMOS camera, and weather stations at both nodes. All measurements are time-stamped, stored in structured log files, and synchronized with the *iPerf* throughput data for post-analysis. The software also implements automatic safety and diagnostic functions: it monitors for link interruptions, amplifier faults, and temperature anomalies, and triggers predefined recovery actions such as amplifier shutdown or alignment reinitialization. Through asynchronous communication channels, each terminal periodically reports its operational state to a central monitoring dashboard that provides visual feedback on link health and power evolution in real time. In extended outdoor operation, the network-based architecture further enables remote management and off-site supervision of both terminals. This capability is particularly

valuable during adverse weather or nighttime experiments, where physical access to the telescope housings is limited. All collected data are synchronized over secure channels to ensure integrity and continuity throughout multi-day field trials.

Our integrated control framework significantly improves the reliability and maintainability of long-range FSOC links. By decoupling hardware control from experimental logic, the *AraOptical* software framework enables flexible experimentation, supports remote configuration, and minimizes manual intervention during multi-hour tests. Moreover, its event-driven design allows future integration with advanced supervisory algorithms for adaptive gain control and predictive alignment. Overall, the inclusion of a programmable software layer elevates the *AraOptical* system from a hardware demonstration to a scalable and reproducible research platform for autonomous optical communication experiments.

III. Results and Discussions

A. Performance Characterization of COTS SFP+ Transceivers

To comprehensively evaluate the performance of *AraOptical* system under real-world operating conditions, we examine the behavior of COTS 10G SFP+ transceivers in our 10.15 km FSOC link. To capture the system's real-time throughput performance, *iPerf* tests were conducted continuously to measure the effective bit rate based on User Datagram Protocol (UDP), which prevents complete channel dropouts caused by power fluctuations. Since the link was established, we have recorded a peak effective bit rate of 2.92 Gbps in the *iPerf* test over a single-channel 10G SFP+ transceiver. The reduced effective bit rate is mainly caused by the use of COTS transceivers, which are designed for relatively stable fiber links and therefore have limited tolerance to the strong and fast power fluctuations encountered in free-space channels. The rapidly varying power fluctuations trigger an internal clock re-synchronization, during which package loss and bit errors will occur. Although these re-synchronization intervals are short, they significantly reduce the effective bit rate.

The time-domain measurement of received optical power, shown in Fig. 4, illustrates the temporal fluctuations for both amplified and unamplified configurations over a four-hour continuous experiment. The amplified channel exhibits higher received power levels, but also experiences a broader dynamic range of approximately 15 dB due to the combined effects of optical amplifier gain dynamics and enhanced sensitivity to atmospheric turbulence. In contrast, the unamplified channel maintains lower yet relatively stable power levels, operating consistently near the receiver sensitivity threshold. Two noticeable power interruptions correspond to automatically detected link-down events, triggered by the preset internal protection mechanism. During these periods, the transceiver was momentarily overwhelmed by the large instantaneous optical power fluctuations, which exceeded its linear operating range and caused the loss of temporal synchronization between the transmitting and receiving modules. As a result, the algorithm initiated an autonomous reboot sequence to restore clock recovery and data alignment before normal communication resumed. These observations indicate that while optical amplification significantly improves the link margin, it also introduces higher susceptibility to dynamic instability, highlighting the trade-off between received power enhancement and link robustness in long-distance FSO systems.

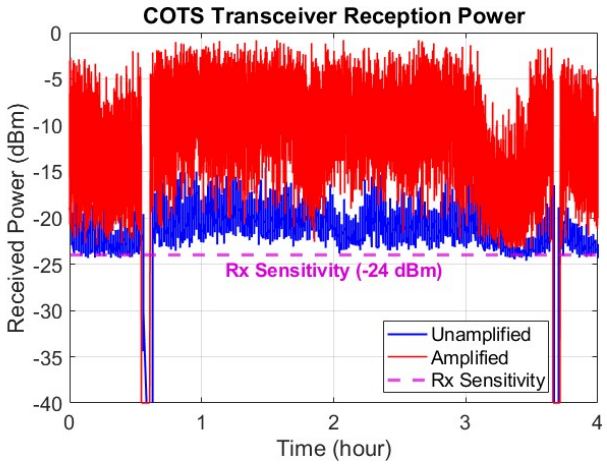

Fig. 4. Four-hour measurement of received optical power for COTS transceivers with and without LNA amplification.

To quantify the strength of atmospheric turbulence, the scintillation index σ_I^2 is defined as the normalized variance of the received irradiance fluctuations, as:

$$\sigma_I^2 = \frac{\langle I^2 \rangle - \langle I \rangle^2}{\langle I \rangle^2} \tag{1}$$

Here, I denotes the irradiance of the optical wave and the angle brackets $\langle \cdot \rangle$ represent long-time average. By evaluating σ_I^2 from the measured power fluctuations, we directly quantify the turbulence-induced intensity variations along the link.

Here, the atmospheric turbulence is quantified by the refractive index structure parameter C_n^2, which describes the magnitude of random refractive index fluctuations caused by temperature and pressure inhomogeneities. It can be expressed as

$$C_n^2 = \frac{\sigma_R^2}{1.23\, k^{7/6}\, L^{11/6}}, \tag{2}$$

where $k = 2\pi/\lambda$ is the optical wave number, λ is the wavelength, and L is the propagation path length. In the weak fluctuation regime ($C_n^2 \leq 10^{-15} m^{-2/3}$), the scintillation index σ_I^2 is statistically equivalent to the Rytov variance σ_R^2 and is, therefore, used as an empirical reference for turbulence characterization. Larger values of σ_R^2 correspond to stronger turbulence and lead to increased scintillation index values, which directly transfer to higher received power fluctuations and degraded link performance in the FSOC system. However, for strong turbulence conditions ($\sigma_I^2 > 1$), σ_I^2 saturates and no longer equals σ_R^2; in such cases, C_n^2 is obtained by numerically solving the generalized scintillation expression that links σ_I^2 and σ_R^2 [7]. In addition to scintillation-induced intensity fluctuations, beam wander was also observed in the long-distance field deployment. CMOS camera measurements indicate angular variations in the beam arrival direction on the order of 30.2 µrad, corresponding to a lateral displacement of approximately 30 cm at a 10 km propagation distance, which

remains within the error that can be compensated by the 1 m beam size at the receiver. Also, beam wandering primarily contributes to slow, low-frequency amplitude variations that might be addressed by the LNA.

In the experiment, the received optical power was continuously logged at the fast Power Meter (PM), enabling the calculation of the Rytov variance from real-time measurements, based on equation (1) . The 2-hour continuous transmission data were segmented into one-minute blocks. For each block, the mean received power and the corresponding average bit rate were calculated. This granularity enables correlation of link performance with atmospheric turbulence metrics, such as Rytov variance, to better understand the relationship between physical layer impairments and communication quality.

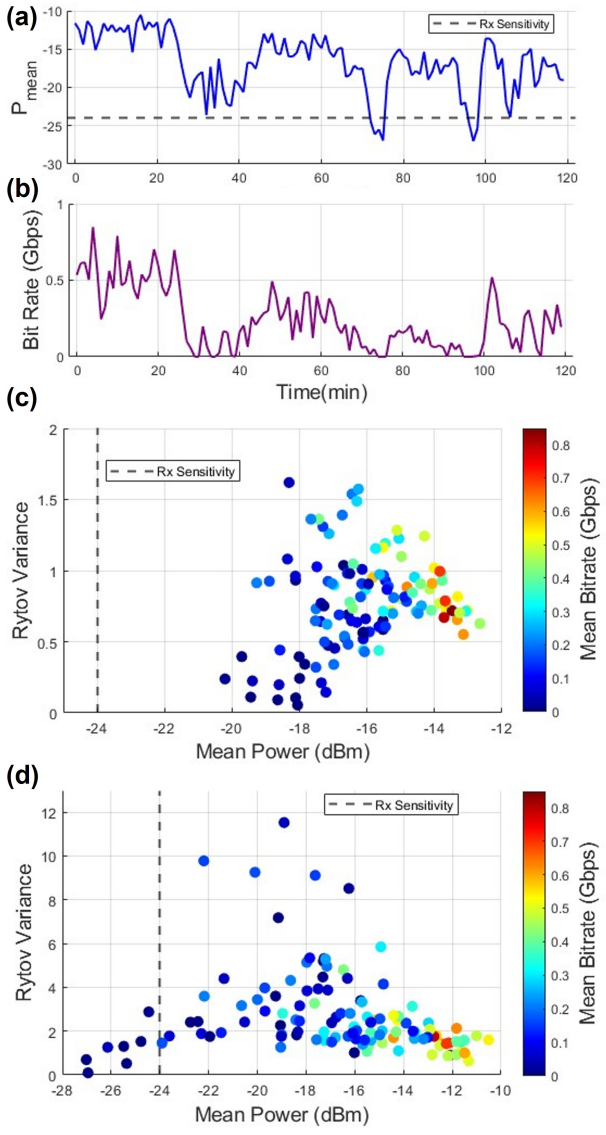

Fig. 5. Performance analysis of the *AraOptical* FSOC link: (a) minute-wise mean reception power at transceiver Rx; (b) minute-wise mean bit rate;(c) Histogram of mean effective bit rate as a function of unamplified received power and Rytov variance, generated from one-minute block-averaged measurements. (d) Histogram of mean effective bit rate as a function of LNA-amplified received power and Rytov variance, generated from one-minute block-averaged measurements.

Fig. 5(a) shows the temporal evolution of the received optical power over 2 hours, sampled at the transceiver reception channel. Significant fluctuations are observed, with periods approaching or even dropping below the transceiver sensitivity threshold. The corresponding real-time effective bit rate measured is depicted in Fig. 5(b). Clear performance degradation is evident, with bit rate drops closely correlated with periods of reduced received power. To quantitatively investigate the impact of atmospheric turbulence on link performance, the relationship between received optical power, Rytov variance (as a turbulence indicator), and effective bit rate was analyzed. Moreover, Figs. 5(c) and 5(d) present histogram-based results constructed from one-minute block-averaged measurements, where each histogram bin represents the statistical distribution of the mean effective bit rate conditioned on the corresponding received power and Rytov variance. As shown in Fig. 5(d), a higher mean received power generally results in improved system performance, as evidenced by a positive correlation between bit rate and received power within the operational range. In particular, when the received power exceeds approximately -15 dBm, the system achieves mean bit rates above 0.5 Gbps more consistently. Moreover, even under favorable power conditions, an increase in Rytov variance (> 6) correlates with reduced bit rate, underscoring the impact of turbulence-induced power fluctuations. Additionally, it is indicated by the comparison between Fig. 5(c) and Fig. 5(d), the integration of LNA not only amplifies the received signal but also accentuates the instantaneous power fluctuations caused by turbulence. Importantly, this does not indicate a physical enhancement of atmospheric turbulence, but rather reflects a measurement-domain effect: the LNA amplifies both the signal and the associated electrical noise, thereby increasing the apparent short-term power fluctuations when operating near the receiver sensitivity limit. The LNA operates in automatic power control (APC) mode to maintain a constant average output power; however, the feedback loop response time is on the order of tens of milliseconds, limiting effective suppression to low-frequency fluctuations below approximately 10 Hz. As a result, while amplification and residual circulator leakage increase the average received power above the sensitivity threshold and improve overall system performance, faster fluctuations requiring close to kHz-level response remain uncompensated, leading to an increased dynamic range of short-term power variations at the transceiver reception [17]. Such fluctuations overwhelm the receiver circuits and lead to channel dropout. Future work will investigate the effect of the LNA by implementing and analyzing an automatic gain control (AGC) algorithm operating at 1 kHz to better understand its influence on the observed Rytov variance.

In addition to turbulence-induced power fluctuations, the synchronization behavior of commercial transceivers further affects link stability. Large instantaneous fades can drive the receiver into repeated re-synchronization cycles, during which data transfer is momentarily interrupted. As a result, throughput degradation is not only determined by the mean received power or scintillation strength, but also by the time required for transceivers to re-establish clock and data recovery. In our experiments, we observed that deep fading events were

frequently followed by prolonged recovery intervals, leading to extended periods of reduced bit rate even after the received power returned above the sensitivity threshold. This behavior underscores the coupled impact of turbulence and transceiver dynamics on the overall link availability. To better quantify this coupling and correlate environmental conditions with observed signal fluctuations, the turbulence strength and its impact on the achievable bit rate are analyzed.

B. Atmospheric Turbulence Modeling and Bit rate Prediction

Atmospheric conditions exert a significant influence on FSOC link performance. During the 2-hour transmission session, meteorological data—including temperature, relative humidity, pressure, and wind speed—were continuously collected, as illustrated in Fig. 6. These parameters were selected because they directly influence refractive index fluctuations in the near-ground atmosphere, a relationship that has been widely discussed in the literature [7], [21], [22], [23]. They serve as essential inputs for estimating and modeling the refractive index structure parameter C_n^2, which characterizes turbulence strength and directly impacts signal fading, phase front distortion, and received power fluctuations. In contrast to the measurement-based calculation described in Section III-A, the predicted C_n^2 values in this section are obtained exclusively from measured meteorological parameters (temperature, humidity, pressure, and wind speed), without using any received optical power information [17], [23], [24]. Specifically, C_n^2 and Rytov variance derived from received power fluctuations is used only as reference measurements for turbulence characterization. This design choice is motivated by the practical requirements of real-time link performance prediction in operational FSOC systems. Meteorological parameters can be continuously monitored and are independent of the optical hardware configuration and alignment state. As a result, weather-based turbulence prediction enables real-time predictive estimation of link quality and achievable bit rate, even when the received optical power is not yet available due to other factors such as pointing errors.

Existing turbulence prediction models such as HV [25], PAMELA [24], and Troy [21] were applied to predict C_n^2, and their outputs were compared with empirically estimated values derived from received power fluctuations, as shown in Fig. 7. Although these models have been widely adopted in free-space optical literature, considerable deviations were observed in our dataset. This discrepancy underscores a fundamental limitation of conventional models: their dependency on site-specific empirical calibration or assumptions (e.g., boundary layer depth, aerosol content, and wind profiles), which reduces generalizability across different geographic and environmental contexts [26]. Their rigid structure may also prevent them from capturing non-linear or coupled dependencies between atmospheric parameters that are highly location-dependent and time-dependent. To address this constraint, a site-specific, data-driven model was constructed using the collected weather station data. Here, a polynomial regression approach was applied to correlate environmental variables with measured C_n^2, capable of capturing nonlinear interactions among environmental variables, while remaining interpretable and lightweight compared to more complex machine learning methods [26]. As shown in Fig. 7, the data-driven polynomial regression model is compared against conventional physics-based turbulence models, including HV, PAMELA, and Troy, highlighting its improved adaptability under site-specific and time-varying atmospheric conditions. Moreover, as we record data, we also record windspeed, humidity, temperature and pressure. One of the challenges in modeling is the highly dynamic nature of the environment. Due to rapid variations, we have a limited set of data collected under similar weather conditions. Moreover, further training and learning models require larger amounts of data. Based on these considerations, polynomial regression was selected as a practical compromise. It provides greater modeling flexibility than traditional analytical models while remaining sufficiently interpretable and lightweight, which is particularly important given the limited duration of the field dataset. The regression model shown in Fig. 7 shows a coefficient of determination of $R^2 = 89.92\%$. This strong agreement validates the effectiveness of using in-situ environmental data for turbulence estimation, especially in scenarios where fast deployment, geographic variability, or limited calibration time preclude the use of traditional models. Moreover, this approach offers flexibility to retrain or adapt the model as conditions evolve.

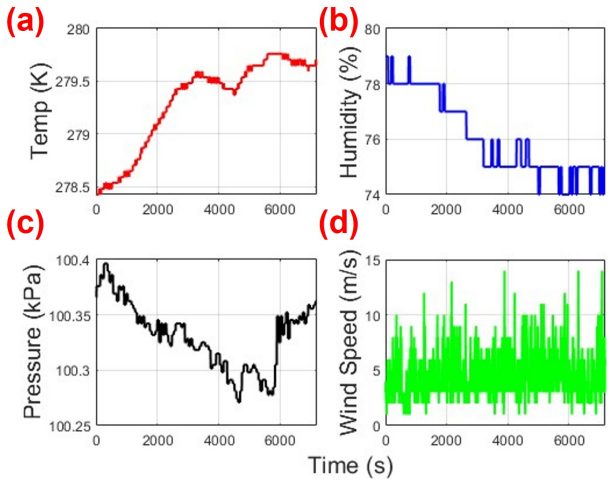

Fig. 6. Weather conditions recorded during the 2-hour FSOC field test: (a) temperature, (b) relative humidity, (c) atmospheric pressure, and (d) wind speed

The predicted C_n^2 values were first used to derive the corresponding predicted Rytov variance. To note, here, the Rytov variance derived from received power fluctuations is used only for validation purposes and is not reused as an input to predict the bit rate. As a result, the predicted Rytov variance and the received power serve as independent inputs to the second-stage polynomial regression model for predicting the effective bit rate and no circular dependency exists in the modeling framework. As shown in Fig. 8, this model achieves a predictive accuracy of $R^2 = 62.22\%$, demonstrating a strong correlation between atmospheric conditions and link-layer performance.

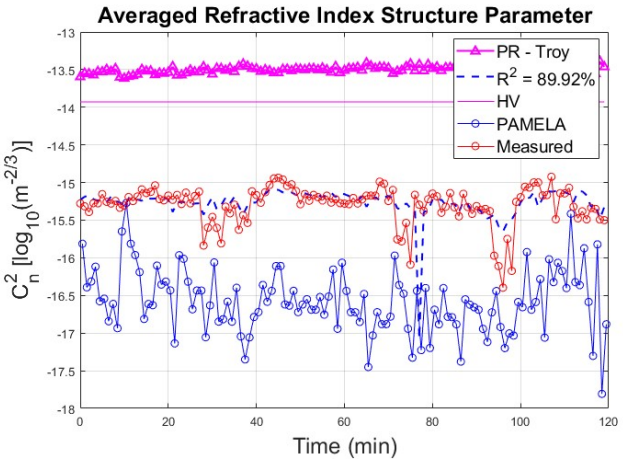

Fig. 7. Comparison of measured and model-predicted refractive index structure parameter C_n^2 during a 2-hour FSOC field test.

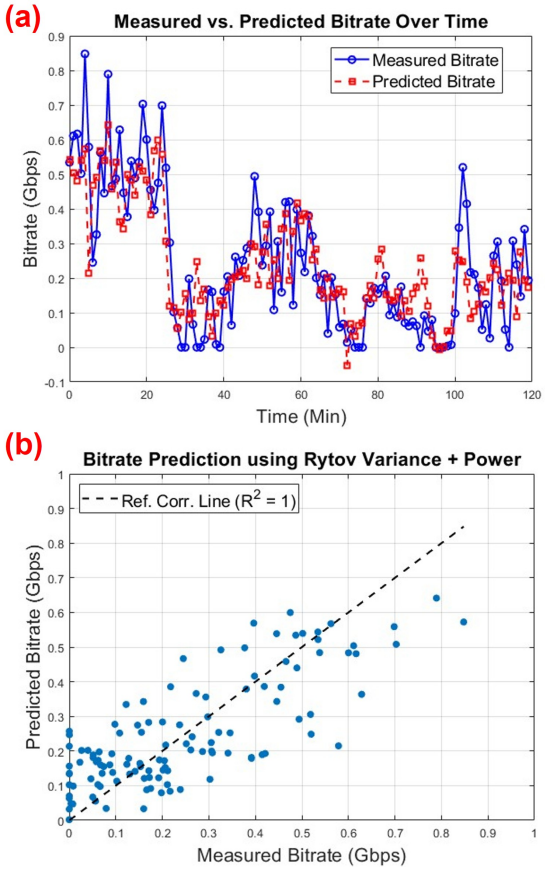

Fig. 8. Bit rate prediction analysis based on turbulence and received power: (a) Comparison of measured and predicted bit rate over time using a regression model with reception power and predicted Rytov variance as predictors; (b) Scatter plot of predicted versus measured bit rate.

Our results establish the feasibility of a fully data-driven pipeline for FSOC performance prediction, where turbulence modeling, power measurements, and throughput estimation can be jointly optimized through environmental sensing. By demonstrating how atmospheric conditions translate into transceiver-level performance limits, our approach provides both fundamental insights into the FSOC system behavior under turbulence and a practical framework for performance prediction tailored to commercial SFP+. Furthermore, the established performance baseline can guide future FSOC-specific transceiver design, offering a benchmark for evaluating system-level enhancements and hardware innovations. While the current polynomial regression model already integrates key environmental parameters such as temperature, humidity, and wind speed, its framework can be further expanded to accommodate higher-order or interaction terms, as well as additional sensing modalities. For instance, incorporating features derived from real-time image-based visibility estimation could refine the turbulence characterization and improve prediction accuracy under rapidly changing atmospheric conditions. Such extensions would enable a more comprehensive understanding of the link adaptation dynamics and facilitate proactive control strategies for future FSOC systems.

While the proposed model provides a grounded framework for weather-based turbulence prediction, it is worth mentioning that its statistical validation is subject to the practical constraints of variable, long-term field experimentation. In particular, the limited number of continuous measurement periods and the strong temporal variability of atmospheric conditions restrict the applicability of conventional data-driven validation strategies until an extensive amount of data can be collected. As part of a publicly accessible research infrastructure, the testbed is expected to facilitate broader community participation and support the collection of larger and more diverse datasets for future model training and development.

IV. Conclusion

In this work, we demonstrated the design, deployment, and characterization of *AraOptical*, a 10.15 km rural FSOC system constructed using COTS 10G SFP+ transceivers. Field experiments showed that the system achieved a peak effective bit rate of 2.92 Gbps and sustained transmission over two hours despite atmospheric turbulence and power fluctuations.

A detailed performance analysis revealed that when the mean received power exceeded -15 dBm, the system maintained bit rates above 0.5 Gbps with high consistency. However, high turbulence—quantified by Rytov variance exceeding 6—resulted in significant degradation, occasionally driving the bit rate to near-zero, even under favorable power levels. Additionally, the presence of a LNA was shown to enhance received signal strength, however, simultaneously amplify instantaneous power fluctuations, effectively increasing the observed Rytov variance and stressing the transceiver's dynamic range.

To model the turbulence impact more accurately, a location-specific polynomial regression model was developed using weather station inputs (temperature, humidity, pressure, and wind speed), yielding a turbulence estimation accuracy of $R^2 = 89.92\%$. In the second stage, the predicted C_n^2 and received power were used to forecast link throughput via a regression model that achieved a prediction accuracy of $R^2 = 62.22\%$. These results confirm the feasibility of leveraging in-situ environmental sensing and data-driven modeling

to quantitatively predict FSOC link performance and enable real-time link adaptation strategies, especially when using COTS transceivers. This is particularly important because standard COTS SFP+ modules are not equipped with forward error correction (FEC), and therefore rely solely on physical-layer signal stability to sustain link integrity. Strong FEC can mitigate packet losses due to turbulence-induced deep fades by trading additional redundancy for improved error resilience, thereby improving the effective throughput. However, these SFP+ modules are primarily designed for short-reach and fiber-optic communication, where the channel is relatively stable and packet-level error rates are typically low. As a result, strong FEC schemes commonly used in long-haul or coherent optical systems are not available in the employed hardware.

Future work will extend the *AraOptical* framework toward multi-node optical mesh networking and adaptive gain control based on real-time turbulence estimation. The modular hardware and software design also allows integration with coherent transceivers and AI-based alignment controllers. However, it is worth mentioning that the integration of AI may increase system complexity. To manage the trade-offs between this added complexity and the need for real-time control, a hybrid architecture can be proposed for future deployment, where the ultrafine alignment algorithm is enhanced by an AI-based decision maker. Instead of directly driving the actuators, the AI agent updates the control parameters (such as step size, scan range, or decision thresholds) of the execution level based on environmental conditions. This approach balances system adaptability with responsiveness, paving the way for fully autonomous optical wireless backhaul systems and enhancing the long-term robustness of next-generation FSOC infrastructures.

REFERENCES

[1] H. Kaushal and G. Kaddoum, *Optical wireless communications: system and channel modelling with MATLAB*. CRC press, 2017.

[2] V. W. S. Chan, "Free-space optical communications," *Journal of Lightwave Technology*, vol. 24, no. 12, pp. 4750–4762, Dec. 2006.

[3] A. Trichili, M. A. Cox, B. S. Ooi, and M.-S. Alouini, "Roadmap to free space optics," *Journal of the Optical Society of America B*, vol. 37, no. 11, pp. A184–A201, Aug. 2020.

[4] H. Hemmati, *Deep Space Optical Communications*. Wiley-Interscience, 2006.

[5] M. Elamassie and M. Uysal, "Free space optical communication: An enabling backhaul technology for 6G non-terrestrial networks," *Photonics*, vol. 10, no. 11, p. 1210, Oct. 2023.

[6] X. Zhu and J. Kahn, "Free-space optical communication through atmospheric turbulence channels," *IEEE Transactions on Communications*, vol. 50, no. 8, pp. 1293–1300, Aug. 2002.

[7] L. C. Andrews and R. L. Phillips, *Laser Beam Propagation through Random Media*, 2nd ed. Bellingham, WA: SPIE Press, 2005.

[8] M. Vargemidou, C. Vagionas, A. Kokkinis, A. Ntanos, A. Stathis, P. Kourelias, G. Giannoulis, H. Avramopoulos, K. Siozios, N. Pleros, and A. Miliou, "Field trial of a SDN-controlled, hybrid FiWi FSO/mmWave x-haul with zero-touch handovers and record-high data rate for 6G," *Journal of Lightwave Technology*, vol. 43, no. 18, pp. 8761–8769, Jul. 2025.

[9] A. K. Majumdar and J. C. Ricklin, *Free-Space Laser Communications: Principles and Advances*. Springer, 2014.

[10] M. A. Khalighi and M. Uysal, "Survey on free space optical communication: A communication theory perspective," *IEEE Communications Surveys & Tutorials*, vol. 16, no. 4, pp. 2231–2258, Jun. 2014.

[11] F. Moll, "Experimental analysis of channel coherence time and fading behavior in the LEO-ground link," in *Proceedings of the International Conference on Space Optical Systems and Applications (ICSOS) 2014*, May 2014.

[12] Coherent Corp., "Coherent announces general availability of 800G ZR/ZR+ in a QSFP-DD form factor," https://www.coherent.com/news/press-releases/general-availability-of-800g-zr-zrplus-in-qsfp-dd-form-factor, Mar. 2025, press Release.

[13] A. J. Vallance, M. Main, M. L. Salloum, M. Dindar, U. J. Daly, P. Ginster, M. A. Cox, and M. P. J. Lavery, "Dynamic aperture selection for turbulence resilience," *IEEE Photonics Technology Letters*, Jun. 2025.

[14] Z. Htay, C. Guerra-Yáñez, Z. Ghassemlooy, S. Zvanovec, M. M. Abadi, and A. Burton, "Experimental real-time GbE MIMO FSO under fog conditions with software defined GNU radio platform-based adaptive switching," *Journal of Optical Communications and Networking*, vol. 14, no. 8, pp. 629–637, Aug. 2022.

[15] R. Jin, J. Ding, M. Xu, S. Chen, M. Zhou, Y. Yu, X. Yan, N. Chi, M. Pu, and X. Luo, "Self-adaptive all-optical feedback-based free- space optical communication system with attention-enhanced turbulence awareness," *Journal of Lightwave Technology*, vol. 43, no. 16, pp. 7605–7616, Aug. 2025.

[16] J. Liu, P. Wang, X. Zhang, Y. He, X. Zhou, H. Ye, Y. Li, S. Xu, S. Chen, and D. Fan, "Deep learning based atmospheric turbulence compensation for orbital angular momentum beam distortion and communication," *Optics Express*, vol. 27, no. 12, pp. 16 671–16 688, Jun. 2019.

[17] M. A. Fernandes, G. M. Fernandes, B. T. Brandao, M. M. Freitas, N. Kaai, and A. Tomeeva, "4 Tbps+ FSO field trial over 1.8 km with turbulence mitigation and FEC optimization," *Journal of Lightwave Technology*, vol. 42, no. 11, pp. 4060–4067, Jun. 2024.

[18] T. U. Islam, J. O. Boateng, M. Nadim, G. Zu, M. Shahid, X. Li, T. Zhang, S. Reddy, W. Xu, A. Atalar, V. Lee, Y.-F. Chen, E. Gossling, E. Permatasari, C. Somiah, O. Perrin, Z. Meng, R. Afzal, S. Babu, M. Soliman, A. Hussain, D. Qiao, M. Zheng, O. Boyraz, Y. Guan, A. Arora, M. Y. Selim, A. Ahmad, M. B. Cohen, M. Luby, R. Chandra, J. Gross, K. Keahey, and H. Zhang, "Design and implementation of ara wireless living lab for rural broadband and applications," *Computer Networks*, vol. 263, p. 111188, May 2025.

[19] X. Li *et al.*, "Design and prototype of auto-track long-range free-space optical communication," in *Optical Fiber Communication Conference (OFC) 2022*. Optica Publishing Group, Apr. 2022, paper W2A.30.

[20] M. Nadim, X. Li, S. Reddy, S. Babu, A. Ahmad, O. Boyraz, D. Qiao, A. Arora, and H. Zhang, "AraOptical system and testbed for long-range, high-capacity FSOC in rural wireless x-haul networks," vol. 3, no. CoNEXT4, Dec. 2025, pp. 39:1–39:21.

[21] T. T. Leclerc, R. L. Phillips, L. C. Andrews, D. T. Wayne, and P. S. andRobert Crabbs, "Prediction of the ground-level refractive index structure parameter from the measurement of atmospheric conditions," in *Atmospheric Propagation VII*. Proc. SPIE, May 2010, p. 76850A.

[22] R. Barrios and V. F. Dios, "Wireless optical communications through the turbulent atmosphere: A review," in *Optical Communications Systems*. InTech — Open Access Company, Mar. 2012, pp. 3–40.

[23] D. Sadot and N. S. Kopeika, "Forecasting optical turbulence strength on the basis of macroscale meteorology and aerosols: models and validation," *Optical Engineering*, vol. 31, pp. 200–212, Feb. 1992.

[24] S. Doss-Hammel, E. Oh, J. C. Ricklin, F. D. Eaton, G. C. Gilbreath, and D. Tsintikidis, "A comparison of optical turbulence models," in *Free-Space Laser Communications IV*. Proc. SPIE, Oct. 2004, p. 5550.

[25] J. W. Strohbehn, *Laser Beam Propagation in the Atmosphere*. Springer Berlin, Heidelberg, 1990.

[26] U. Celik, H. A. Yasar, C. B. Merve Yigitoglu Keskin, I. Aslantas, and Y. Midilli, "Estimation of ground-based atmospheric turbulence strength (C_{n}^2) by neural network architecture," *Applied Optics*, vol. 63, pp. 7402–7409, Oct. 2024.